1521-0111/12/8206-1183–1193$25.00
MOLECULAR PHARMACOLOGY
Copyright © 2012 The American Society for Pharmacology and Experimental Therapeutics
Mol Pharmacol 82:1183–1193, 2012

Vol. 82, No. 6
80176/3806685

Cd^{2+} Block and Permeation of $Ca_V3.1$ (α1G) T-Type Calcium Channels: Candidate Mechanism for Cd^{2+} Influx

Kyle V. Lopin, Frank Thévenod, Jessica C. Page, and Stephen W. Jones

Department of Physiology and Biophysics, Case Western Reserve University, Cleveland, Ohio (K.V.L., S.W.J.); Center for Biomedical Research and Education, Institute for Physiology and Pathophysiology, Witten/Herdecke University, Witten, Germany (F.T.); and University of Buffalo, Buffalo, New York (J.C.P.)

Received May 22, 2012; accepted September 11, 2012

ABSTRACT

Cd^{2+} is an industrial pollutant that can cause cytotoxicity in multiple organs. We examined the effects of extracellular Cd^{2+} on permeation and gating of $Ca_v3.1$ (α1G) channels stably transfected in HEK293 cells, by using whole-cell recording. With the use of instantaneous I-V currents (measured after strong depolarization) to isolate the effects on permeation, Cd^{2+} rapidly blocked currents with 2 mM Ca^{2+} in a voltage-dependent manner. The block caused by Cd^{2+} was relieved at more-hyperpolarized potentials, which suggests that Cd^{2+} can permeate through the selectivity filter of the channel into the cytosol. In the absence of other permeant ions (Ca^{2+} and Na^+ replaced by *N*-methyl-D-glucamine), Cd^{2+} carried sizable inward currents through $Ca_v3.1$ channels (210 ± 20 pA at −60 mV with 2 mM Cd^{2+}). $Ca_v3.1$ channels have a significant "window current" at that voltage (open probability, ~1%), which makes them a candidate pathway for Cd^{2+} entry into cells during Cd^{2+} exposure. Incubation with radiolabeled $^{109}Cd^{2+}$ confirmed uptake of Cd^{2+} into cells with $Ca_v3.1$ channels.

Introduction

Increasing industrial use of Cd^{2+} has led to widespread contamination of the environment, which threatens human health (Agency for Toxic Substances and Disease Registry, 2008). The main challenge in the 21st century, from a global perspective, seems to be not acute toxicity but chronic, low-level, Cd^{2+} exposure, mainly from dietary sources (Järup and Akesson, 2009). The ubiquity of Cd^{2+} makes it a serious environmental health problem that needs to be assessed thoroughly, because it affects, or will affect, large proportions of the world's population.

A variety of pathways to allow Cd^{2+} entry into excitable and nonexcitable cells have been suggested (Thévenod, 2010). Candidates include divalent metal ion transporter 1, with a K_m for Cd^{2+} of ~1 μM (Gunshin et al., 1997; Okubo et al., 2003), ZIP8, with a K_m for Cd^{2+} of ~0.5 μM (Liu et al., 2008), and ZIP14A/B, with a K_m for Cd^{2+} of 0.1 to 1 μM (Girijashanker et al., 2008). It is crucial to note that blood Cd^{2+} concentrations are in the range of 1 to 10 nM in the general population (Elinder et al., 1983) and may exceed 100 to 300 nM among occupationally exposed workers (Hassler et al., 1983). The free Cd^{2+} concentrations in the extracellular fluid that cause tissue damage are not known but are likely to be in the submicromolar range; even acute poisoning with oral intake of a high dose of Cd^{2+} results in Cd^{2+} concentrations in the blood of merely ~200 nM (Hung and Chung, 2004). It is not clear whether most studies describing Cd^{2+} transport have only in vitro or mechanistic relevance or indicate significant contributions to the in vivo toxicity of Cd^{2+}.

T-type calcium channels are blocked by Cd^{2+} (Lacinová et al., 2000; Díaz et al., 2005), but their role in Cd^{2+} transport has not been investigated to date. $Ca_v3.1$ channels may be suitable for Cd^{2+} transport, because they have a well defined window current at negative membrane potentials at which the driving force for divalent cation entry is high (Serrano et al., 1999) and they are ~2-fold less selective for Ca^{2+} than are L-type calcium channels (Perez-Reyes, 2003), which suggests that Cd^{2+} has an increased chance of permeating the channel in the presence of competing Ca^{2+}. $Ca_V3.1$ channels are expressed in excitable cells, such as neurons and heart, smooth and skeletal muscle, and endocrine cells (Perez-Reyes, 2003). $Ca_v3.1$ channels also are expressed in the distal nephrons of the kidney (Andreasen et al., 2000), where it may be involved in Ca^{2+} reabsorption (Leclerc et al., 2004). In this

This work was supported in part by the Deutsche Forschungsgemeinschaft [Grant TH345/11-1] and the Stiftung Westermann-Westdorp.
K.V.L. and F.T. contributed equally to this work.
Article, publication date, and citation information can be found at http://molpharm.aspetjournals.org.
http://dx.doi.org/10.1124/mol.112.080176.

ABBREVIATIONS: ZIP, Zrt- and Irt-like protein; HBSS, Hanks' balanced salt solution; NMDG, *N*-methyl-D-glucamine; GHK, Goldman-Hodgkin-Katz; $[Cd^{2+}]_o$, extracellular Cd^{2+} concentration; NNC 55-0396, (1*S*,2*S*)-2-(2-(*N*-[(3-benzimidazol-2-yl)propyl]-*N*-methylamino)ethyl)-6-fluoro-1,2,3,4-tetrahydro-1-isopropyl-2-naphtyl cyclopropanecarboxylate dihydrochloride.

study, we examined the effects of Cd^{2+} on the gating and permeation of $Ca_v3.1$ channels, and we used a model of permeation to estimate the amounts of Cd^{2+} that can permeate through the channels at levels seen during chronic Cd^{2+} exposure.

Materials and Methods

Electrophysiological Studies. Whole-cell patch-clamp recordings were made from HEK293 cells stably transfected with $Ca_V3.1$ calcium channels, as described previously (Khan et al., 2008). Electrodes were made from borosilicate glass (World Precision Instruments, Sarasota, FL) and had open-tip resistances of 1.1 to 2.0 MΩ and access resistances under whole-cell conditions of 2.0 to 5.0 MΩ. Currents were recorded at room temperature (~21–24°C), compensated at 90%, filtered at 10 kHz, and sampled at 50 kHz. Leak and capacitative currents were subtracted by using a −P/4 protocol. A holding potential of −100 mV was used to prevent inactivation of the channels. Only cells with resting leaks of <200 pA and rundown values of <25% were used. Currents were acquired by using an Axopatch 200A amplifier and pClamp 8.2 software (Molecular Devices, Sunnyvale, CA) and were analyzed by using Clampfit (Molecular Devices) and MATLAB (MathWorks, Natick, MA).

Recording Solutions. The intracellular solution used for all experiments contained 2 mM $CaCl_2$, 1 mM $MgCl_2$, 120 mM NaCl, 10 mM HEPES, 11 mM EGTA, and 4 mM Mg-ATP. The pH was ad-

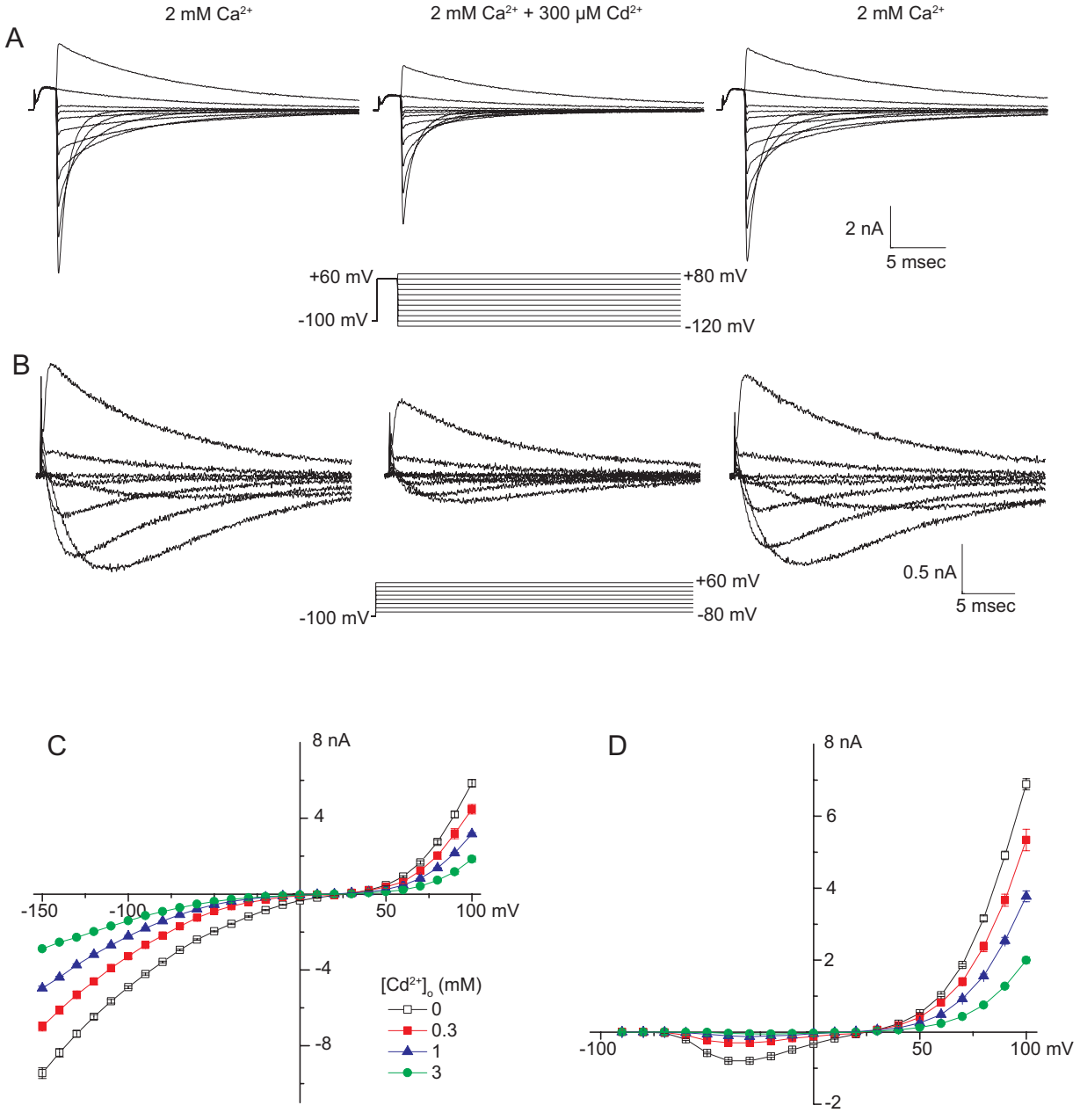

Fig. 1. Cd^{2+} block of currents through $Ca_v3.1$ channels. A and B, sample II-V (A) and I-V (B) records. The protocols are shown below the middle traces. Control currents with 2 mM Ca^{2+} (left), currents with the addition of 300 μM Cd^{2+} (middle), and currents after washout (right) are shown. Currents were Gaussian-filtered offline to a final −3-dB cutoff value of 5 kHz and are shown in 20-mV increments. C, instantaneous currents from the II-V protocols shown in A, under control conditions and in the presence of three concentrations of Cd^{2+} (n = 4 for all concentrations). D, peak currents for the I-V protocol shown in B (n = 4). Symbols definitions for C also apply to D.

justed to 7.2 with NaOH. The free Ca^{2+} concentration was calculated as 70 nM. The standard extracellular solution contained 2 mM $CaCl_2$, 135 mM NaCl, 10 mM HEPES, and 10 mM glucose. The pH was adjusted to 7.2 with NaOH. Where indicated, $CdCl_2$ was added to the extracellular solution. For the Ba^{2+} data, $BaCl_2$ replaced $CaCl_2$. For the data on Cd^{2+} permeation with $NMDG^+$, Na^+ was replaced by $NMDG^+$ and the pH was adjusted with HCl. All chemicals used in the electrophysiological experiments were purchased from Sigma-Aldrich (St. Louis, MO).

Data Analyses. The current through ion channels is affected by two processes, i.e., gating and permeation. To separate these two, we used an "instantaneous" current-voltage (II-V) protocol to isolate the gating of $Ca_v3.1$ from permeation (Hodgkin and Huxley, 1952). The II-V protocol used a short (2-ms) pulse to a voltage that maximally opened the channels (+60 mV). The potential was then reset to different voltages in a wide range, and the initial currents were measured (Fig. 1A). Because the initial pulse opened the same number of channels for each recording, the current-voltage relationship was directly proportional to the permeation of ions through a single channel. To determine the effect of added Cd^{2+} on the II-V relationship ("Cd^{2+} block"), currents were converted to chord conductances (Khan et al., 2008), because Cd^{2+} affected the reversal potential and thus the driving force at a particular voltage.

In a second protocol (I-V), steps from the holding potential to different depolarizing potentials were applied, and the currents were recorded (Fig. 1B). The currents recorded with the I-V protocol were affected by both gating and permeation. Dividing the I-V current by the II-V current for each voltage yielded the relative open probability (Serrano et al., 1999).

Inward currents with Cd^{2+} as the charge carrier were too small to measure. To measure any change in gating under those conditions, channels were activated with a short (2-ms) pulse to different voltages and tail currents were measured after the potential was reset to −100 mV. Because the driving force for the tail currents was the same for each recording, any difference in the currents would be proportional to the number of channels opened during the 2-ms voltage step.

For Cd^{2+} block, cells were assessed in control solution (2 mM Ca^{2+}), after the addition of Cd^{2+}, and after return to control solution (washout) (Fig. 1, A and B). The control and washout currents were averaged to offset any rundown that might have occurred for data on Cd^{2+} block of Ca^{2+} currents. Averaging of control and washout currents was not performed for Cd^{2+} permeation data, because the cells became very leaky when switched back to Ca^{2+} after being exposed to high levels of Cd^{2+} without Ca^{2+} for periods of >2 min. To evaluate rundown, briefer (~30-s) Cd^{2+} applications were used and tail currents at −100 mV were measured after brief test pulses, before, during, and after recovery from the Cd^{2+} applications. We estimated that currents observed with 10 mM Cd^{2+} were reduced 14 ± 2% through rundown, and there was no significant change with 2 mM Cd^{2+} (data not shown).

In each condition, data were scaled on the basis of the sum of the II-V currents from +80 to −80 mV, to reduce variability resulting from cell-to-cell variations in channel expression (Khan et al., 2008). For the II-V protocol, the initial amplitudes were estimated from fits to a single-exponential equation,

$$= A \cdot e^{-t/\tau} + C$$

where A is the initial amplitude, τ is the time constant of decay, and C is a constant offset. Inward currents for the I-V protocol were too small to be fit accurately to exponential equations for all except the control and 0.3 mM Cd^{2+} conditions. For the I-V data, the peak currents were measured by averaging data between two cursors placed around the peak through visual estimation.

Permeablility Ratios. Reversal potentials were calculated through linear interpretation of data between data points on both sides of the reversal. Permeability ratios were calculated from the reversal potentials on the basis of the Goldman-Hodgkin-Katz (GHK) theory. For two ions,

$$\frac{P_A}{P_B} = \frac{-z_B^2 \cdot ([B]_i - [B]_o e^{-v_B}) \cdot (1 - e^{-v_A})}{z_A^2 \cdot ([A]_i - [A]_o e^{-v_A}) \cdot (1 - e^{-v_B})}$$

where $v_i = z_i V_r F/RT$ (Frazier et al., 2000). With three permeant ions (Cd^{2+}, Ca^{2+}, and Na^+) the following equation can be derived:

$$\frac{P_A}{P_B} = \left[\frac{-P_C \cdot z_C^2 \cdot ([C]_i - [C]_o e^{-v_C}) \cdot (1 - e^{-v_B})}{P_B \cdot z_B^2 \cdot ([B]_i - [B]_o e^{-v_B}) \cdot (1 - e^{-v_C})} - 1 \right] \cdot \left[\frac{z_B^2 \cdot ([B]_i - [B]_o e^{-v_B}) \cdot (1 - e^{-v_A})}{z_A^2 \cdot ([A]_i - [A]_o e^{-v_A}) \cdot (1 - e^{-v_B})} \right]$$

This equation predicts that the addition of a permeant extracellular ion would produce a more-positive reversal potential.

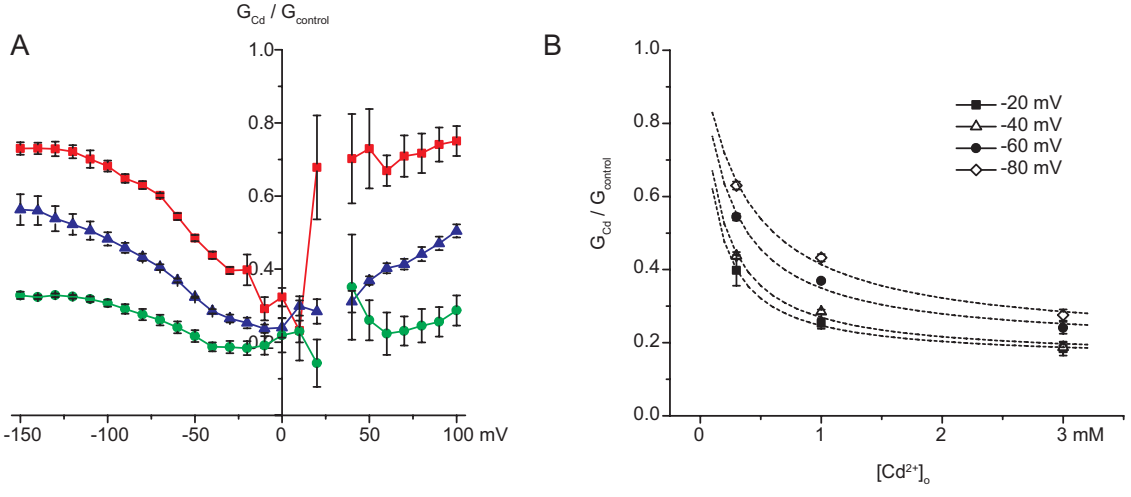

Fig. 2. Fractions of chord conductances remaining with Cd^{2+}. A, ratio of the conductance in the presence of Cd^{2+} to control values as a function of voltage. Data were from II-V measurements as in Fig. 1C (n = 4). Symbols are as defined for Fig. 1C. B, conductance ratios as a function of Cd^{2+} concentrations. Curves are fits to a single-site model with variable maximal inhibition, as follows: 0.11 mM, 84% inhibition (−20 mV); 0.15 mM, 84% inhibition (−40 mV); 0.23 mM, 80% inhibition (−60 mV); 0.36 mM, 80% inhibition (−80 mV). Data were not well described with a single-site model with 100% maximal inhibition.

Gating. To measure the effect of Cd^{2+} on gating, channel activation was measured by fitting currents from the I-V protocol to a fourth-power Boltzmann function,

$$P_{o,r}(V) = \left(\frac{1}{1 + e^{\left(\frac{-(V - V_{0.5})}{k}\right)}}\right)^4$$

where $V_{0.5}$ is the half-point of activation for an individual voltage sensor and k is the voltage sensor sensitivity. Voltage shifts in gating caused by Cd^{2+} were calculated by subtracting the $V_{0.5}$ for Cd^{2+} activation from the average $V_{0.5}$ for control (2 mM Ca^{2+}) and washout conditions (Zhou and Jones, 1995). The equation described by Grahame (1947) was used to calculate voltage shifts resulting from charge screening, according to the Gouy-Chapman theory,

$$\sigma^2 G^2 = \sum [C_i]\left\{e^{\frac{-z\psi}{kT}} - 1\right\}$$

where G is a constant equal to 270 Å^2 e^{-1} M$^{1/2}$ at room temperature, C_i is the concentration of the ith ionic species in solution, z is the valance, k is Boltzmann's constant, T is the temperature, ψ is the observed voltage shift, e is the charge of a proton, M is the molar concentration, and σ is the planar charge density. For charge screening without binding, σ was set to 1 e^-/98 Å^2, as estimated previously (Khan et al., 2008). Binding of Cd^{2+} to the planar charge followed the Gouy-Chapman-Stern theory,

$$\sigma = \sigma_t\left[1 + K_{Cd}[Cd]_o e^{\frac{-z_i\psi}{kT}}\right]^{-1}$$

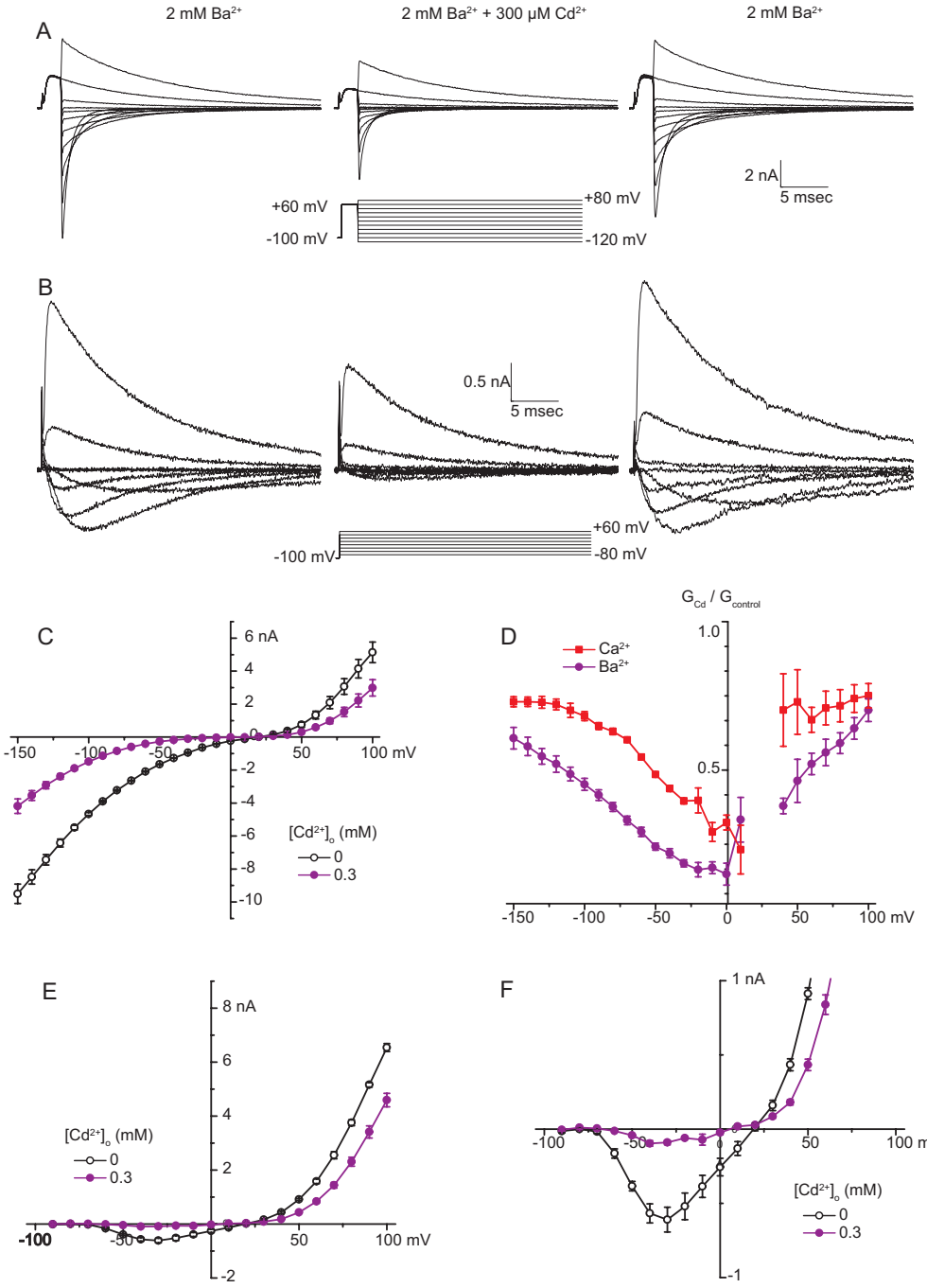

Fig. 3. Cd^{2+} block of Ba^{2+} currents. A and B, II-V (A) and I-V (B) current records, obtained by using the protocols shown below the middle traces. Control currents with 2 mM Ba^{2+} (left), currents with the addition of 300 μM Cd^{2+} (middle), and currents after washout (right) are shown. Currents were Gaussian-filtered at 5 kHz and are shown in 20-mV increments. C, instantaneous currents from the II-V protocol shown in A. D, fractions of control conductances remaining with 300 μM Cd^{2+} when 2 mM Ca^{2+} or Ba^{2+} was the charge carrier. E, peak currents from the I-V protocol shown in B. F, expanded view of the inward currents with the I-V protocol. For experiments with Ba^{2+}, $n = 4$.

where σ_t was set to 1 e^-/98 Å^2, K_{Cd} is the association constant for Cd^{2+}, and σ is the surface charge not neutralized by binding.

Permeation Model. We previously described a two-site/three-barrier Eyring model for $Ca_V3.1$ permeation (Lopin et al., 2010). The II-V data collected in this study were normalized to the original data. The parameters for the electrical distances and the energy parameters for Ca^{2+}, Ba^{2+}, Na^+, and Mg^{2+} were fixed to the parameters fitted previously. Parameters for Cd^{2+} were fitted with a least sum of absolute errors to all of the data points by using the Levenberg-Marquardt algorithm.

$^{109}Cd^{2+}$ Transport. Cellular uptake of $^{109}Cd^{2+}$ (specific activity, 1.5 MBq/μg of Cd^{2+}; QSA Global, Braunschweig, Germany) was assessed according to a previously described protocol (Erfurt et al., 2003), with some modifications. Confluent monolayers of HEK293 cells (control cells or cells stably transfected with $Ca_V3.1$) were washed twice with HBSS with 5.55 mM glucose (HBSS-glucose) before incubation with Cd^{2+}. The concentration of $CdCl_2$ (10 mM stock solution in water) was adjusted with HBSS-glucose, and $^{109}Cd^{2+}$ was added to yield a final activity of 18.5 kBq/ml. At specific time points, monolayers were washed with HBSS-glucose containing 2 mM EGTA (pH 7.0, adjusted with Tris) and were solubilized overnight with 1 N NaOH. $^{109}Cd^{2+}$ contents were determined by using a Cobra II Auto-Gamma counter (PerkinElmer Life and Analytical Sciences, Waltham, MA). Experiments were performed in the absence or presence of 25 μM (1*S*,2*S*)-2-(2-(*N*-[(3-benzimidazol-2-yl)-propyl]-*N*-methylamino)ethyl)-6-fluoro-1,2,3,4-tetrahydro-1-isopropyl-2-naphtyl cyclopropanecarboxylate dihydrochloride (NNC 55-0396) (2.5 mM stock dissolved in water; Sigma-Aldrich), a selective inhibitor of T-type calcium channels (Huang et al., 2004), to determine $Ca_V3.1$-specific $^{109}Cd^{2+}$ uptake. Throughout the article, data are presented as mean ± S.E.M.

Results

Protocol Used. Cd^{2+} is commonly used to block Ca^{2+} currents. To characterize this effect, most studies used voltage steps (Lacinová et al., 2000) and measured current-voltage relationships, but such relationships reflect the simultaneous effects of Cd^{2+} on gating and pore block. To separate these two effects, we used an instantaneous current-voltage protocol in which a short prepulse was applied to open maximally all of the channels, the voltage was instantly reset, and the current was measured (Fig. 1, A and C). With the II-V protocol, the effects of Cd^{2+} on the permeation pathway could be examined apart from its effects on gating.

Evidence that Cd^{2+} Blocks and Permeates through $Ca_V3.1$ Channels. Figure 1, A and B, shows current records obtained with the II-V and I-V protocols under control conditions (2 mM Ca^{2+} with 145 mM Na^+), with the addition of 300 μM Cd^{2+}, and after washout. The large voltage range allowed both outward Na^+ currents and inward currents carried mainly by Ca^{2+} to be measured. The peak currents for each protocol are shown in Fig. 1, C and D, for experiments conducted under control conditions and in the presence of three different concentrations of Cd^{2+} (0.3, 1, and 3 mM). To determine the voltage dependence of block by Cd^{2+}, the chord conductances measured in the presence of Cd^{2+} were divided by the control value (Fig. 2A). It can be clearly seen that, as the cell was hyperpolarized, the fraction of channels blocked by Cd^{2+} decreased. The rate of Cd^{2+} exit out of the pore to the extracellular side slowed as the cell was hyperpolarized, but if the divalent blocker could permeate, then the rate of Cd^{2+} exiting the pore at hyperpolarizing potentials would increase, relieving pore block. As Díaz et al. (2005) noted for Cd^{2+} with $Ca_V3.1$, "Taken together, these results suggest that extreme hyperpolarization appears to attract Cd^{2+} into the cell." Figure 2B shows the conductance as a function of Cd^{2+} concentration and voltage. The block was saturated at ~85%, because an appreciable current was observed with a $[Cd^{2+}]_o$ level of 3 mM. The remaining cur-

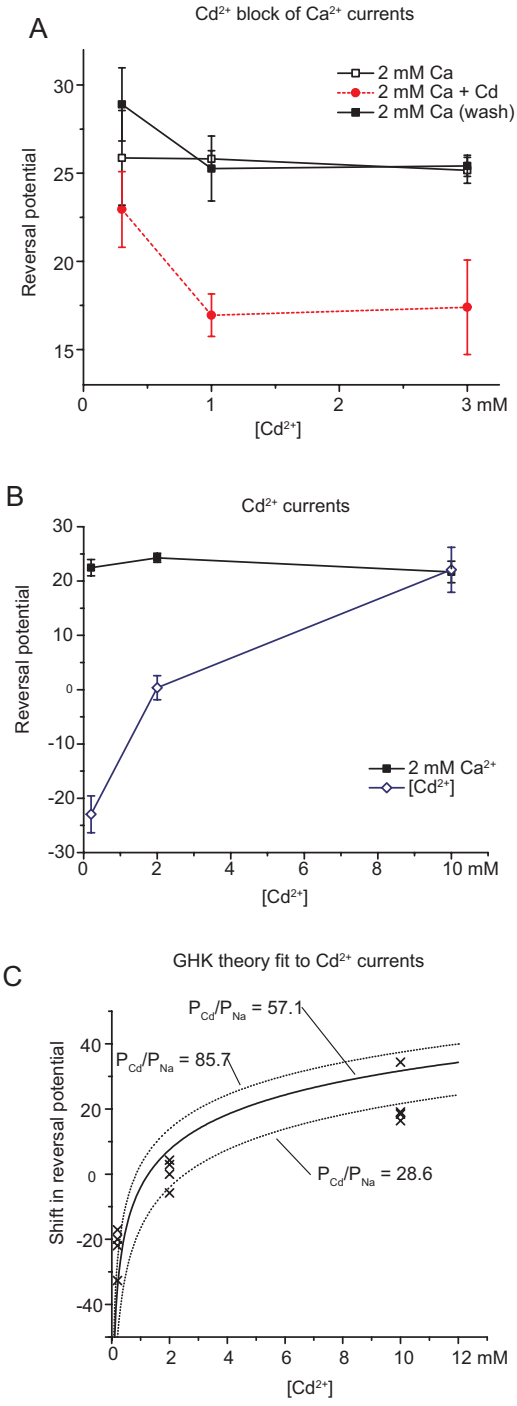

Fig. 4. Effects of Cd^{2+} on reversal potentials. A, effects of the addition of Cd^{2+} (to 2 mM Ca^{2+}) on reversal potentials. B, reversal potentials with extracellular Cd^{2+} (0 mM Ca^{2+} and $NMDG^+$ replacing Na^+ in the extracellular solution) and intracellular Na^+. C, fits of the Cd^{2+}/Na^+ permeability ratio (P_{Cd}/P_{Na}) to the GHK theory. Solid line, best fit (Cd^{2+}/Na^+ permeability ratio of 57.1); dashed lines, GHK fits with the Cd^{2+}/Na^+ permeability ratio increased or decreased by 50% (Cd^{2+}/Na^+ permeability ratios of 85.7 and 28.6, respectively) (n = 4).

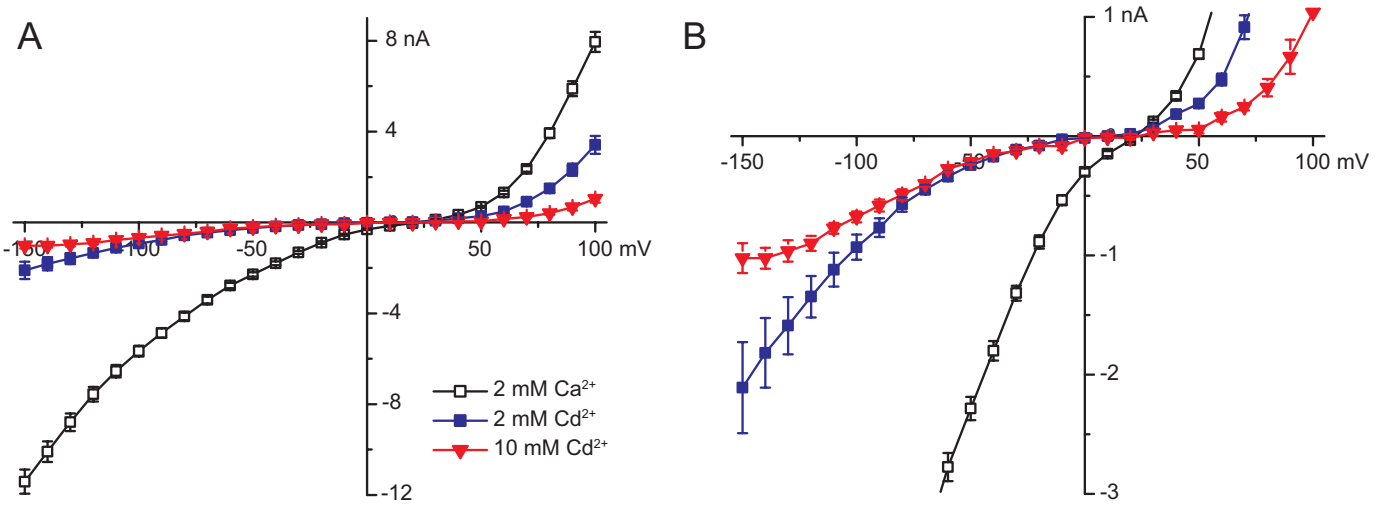

Fig. 5. II-V relationships with extracellular Cd^{2+} and Na^{+}. A, currents recorded when Ca^{2+} was replaced with Cd^{2+}. B, expanded view of data in A. The currents were larger with 2 mM Cd^{2+} than with 10 mM Cd^{2+} at the most hyperpolarized potentials (n = 4).

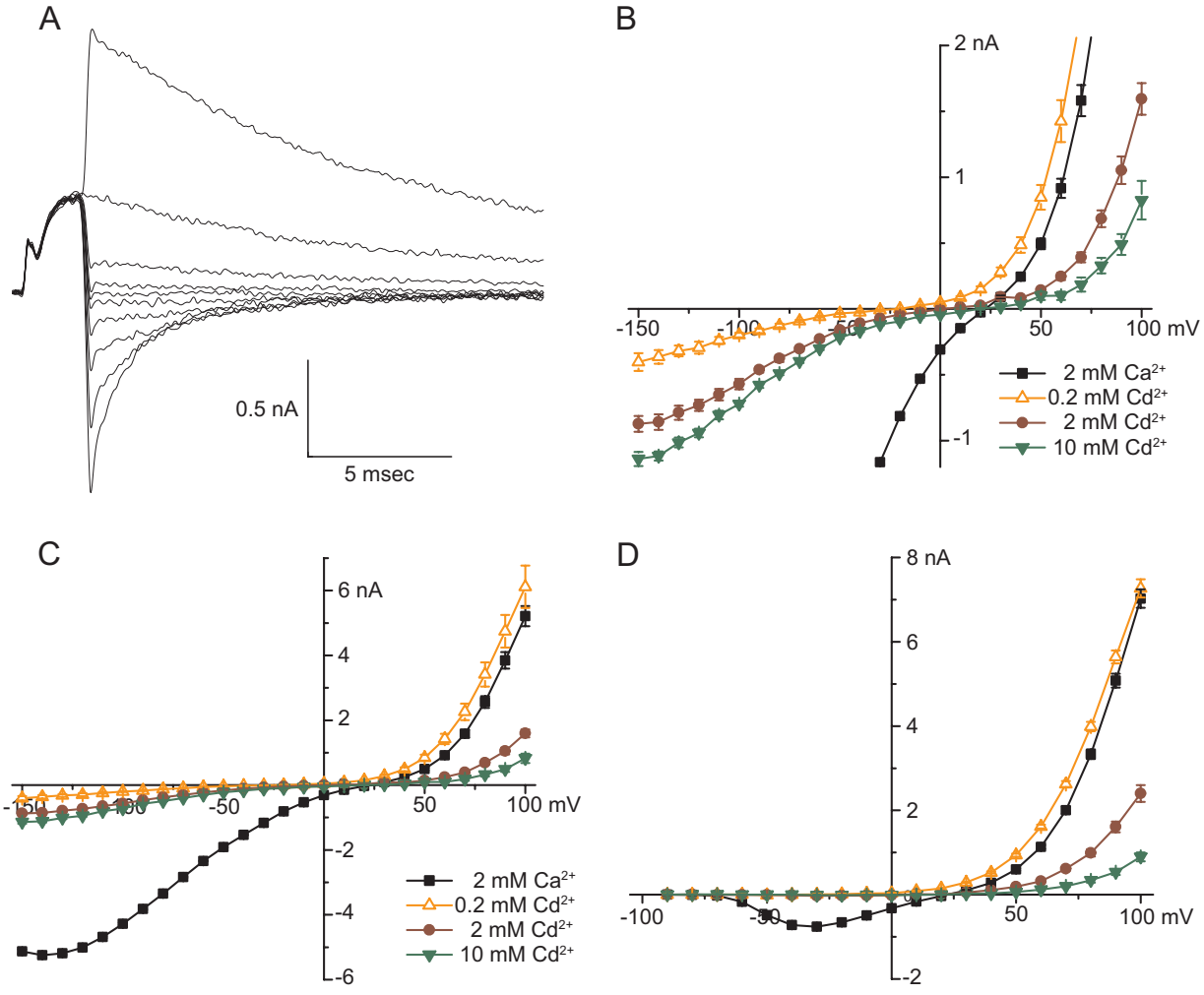

Fig. 6. Permeation by Cd^{2+}. A, sample currents recorded with the II-V protocol with extracellular solution containing 2 mM Cd^{2+} and $NMDG^{+}$. The currents shown were measured between +80 mV and −100 mV in 20-mV increments and are presented after offline, 2-kHz, Gaussian filtering. B, instantaneous currents from the II-V protocol (as in A) presented on an expanded scale, to show inward currents carried by Cd^{2+} (n = 4 for all concentrations). C, same as in B but scaled for comparison of currents carried by Cd^{2+} versus Ca^{2+}. D, peak currents measured by using the I-V protocol (n = 4). Symbols are as in B and C.

rent might be attributable to incomplete block of Ca^{2+} currents and/or Cd^{2+} permeation.

Given the voltage dependence of block, it was likely that Cd^{2+} decreased currents by entering and obstructing the pore. To confirm this, we changed the charge carrier from Ca^{2+} to Ba^{2+} (Fig. 3). It was shown previously (Serrano et al., 2000) that, because of ion-ion interactions in the pore, blockers are more potent when Ba^{2+} is the charge carrier, compared with Ca^{2+}, if the effect of the blocker is on the selectivity filter of the pore. This can clearly be seen in Fig. 3, in which Ba^{2+} currents were blocked appreciably more by 300 μM Cd^{2+} than were Ca^{2+} currents, with either the II-V protocol (Fig. 3, A, C, and D) or the I-V protocol (Fig. 3, B, E, and F).

Because the voltage dependence of block suggested Cd^{2+} permeation, we examined the reversal potentials of the currents after the addition of Cd^{2+}. According to the GHK theory, a permeant ion added on the extracellular side should cause a more-positive reversal potential. As shown in Fig. 4A, addition of Cd^{2+} on the extracellular side actually caused a less-positive reversal potential.

Currents Carried by Cd^{2+}. The voltage dependence of block by Cd^{2+} suggested that Cd^{2+} could permeate through the pore. To test this more directly, we recorded currents after the replacement of 2 mM Ca^{2+} with 2 mM Cd^{2+} (Fig. 5A), and we observed sizeable inward currents (shown on an expanded scale in Fig. 5B). To confirm that the currents observed were being carried by Cd^{2+} and not Na^+, we increased the Cd^{2+} concentration to 10 mM. This did not lead to an increase in the currents, which might be expected if the currents were being carried by Cd^{2+}. At very hyperpolarized potentials (−120 to −150 mV), the current was less with 10 mM Cd^{2+}. One possibility is that some of the inward current is carried by Na^+ and the higher concentration of Cd^{2+} simply blocks the Na^+ current more effectively.

To eliminate any Na^+ currents that might be mixing with the Cd^{2+} currents, we replaced the extracellular Na^+ with $NMDG^+$, an impermeant cation. Figure 6 compares currents with 0.2, 2, and 10 mM Cd^{2+} versus 2 mM Ca^{2+}. Inward currents increased monotonically with the Cd^{2+} concentration, approaching saturation at 10 mM (Fig. 6, B and C). Currents carried by Cd^{2+} were rather large, i.e., >200 pA at −60 mV with $[Cd^{2+}]_o$ levels of both 2 and 10 mM (Fig. 6B). This level of current carried through a calcium channel by a "blocker" is surprising. With the I-V protocol, inward currents were very small (~30 pA) (Fig. 6D). By using the reversal potentials for Cd^{2+} permeation with $NMDG^+$ (Figs. 4B and 6B), the Cd^{2+}/Na^+ permeability ratio was calculated as 57.1 on the basis of the GHK theory (Fig. 4C), which can be compared with the Ca^{2+}/Na^+ permeability ratio of 87 (Khan et al., 2008). This would yield a Cd^{2+}/Ca^{2+} permeability ratio of 0.66, with Cd^{2+} being only slightly less permeable than Ca^{2+}, as defined on the basis of the GHK theory.

Cd^{2+} Uptake through $Ca_V3.1$ Channels. $Ca_V3.1$ channels are known to have a substantial window current, i.e., partial activation combined with incomplete inactivation allows a steady inward Ca^{2+} current near the resting potential (Williams et al., 1997; Serrano et al., 1999; Chemin et al., 2000). The window current is classically measured as the overlap of the activation curve and the inactivation curve; this assumes that inactivation reaches 100% at depolarized potentials. Inactivation is incomplete for $Ca_V3.1$ channels at all potentials, however, and 1 to 3% of channels remain open and conduct current (Serrano et al., 1999). This window current might be an important source of Cd^{2+} entry into cells. To study whether Cd^{2+} could permeate through the window current of $Ca_V3.1$ channels, incubation studies were conducted with radiolabeled $^{109}Cd^{2+}$. Experiments were conducted for 30 min with varying concentrations of Cd^{2+} in the presence of physiological levels of Ca^{2+}. Cd^{2+} uptake by $Ca_V3.1$ channels was measured as the difference between cells incubated with Cd^{2+} and cells incubated with Cd^{2+} and the Ca_V3 blocker NNC 55-0396 (Huang et al., 2004). Figure 7 shows that $Ca_V3.1$ channels could transport Cd^{2+} into cells at the resting membrane potential, in a dose-dependent manner.

Permeation Model. To estimate how $Ca_V3.1$ channels transport trace amounts of Cd^{2+} under physiological conditions, a two-binding site/three-barrier model was used (Fig. 8). Parameters were estimated by fitting the data on Cd^{2+} block and permeation (Figs. 1, 3, and 6). The electrical distances and parameters for Ca^{2+}, Ba^{2+}, Na^+, and Mg^{2+} were fixed to the values used by Lopin et al. (2010). The model was able to describe effectively the Cd^{2+} block of Ca^{2+} currents (Fig. 8A) and Ba^{2+} currents (Fig. 8D) and the permeation of Cd^{2+} (Fig. 8B). However, there was a deviation between the model and the data at the most hyperpolarized potentials (−120 to −150 mV) for Cd^{2+} permeation. When Na^+ was replaced by $NMDG^+$, the current plateaued for potentials less than −120 mV even when Ca^{2+} was the carrier (Khan et al., 2008) (compare control currents in Figs. 6C and 1C). It is unclear whether this was caused by voltage-dependent block of $NMDG^+$ or whether there were Na^+ currents in addition to Ca^{2+} currents at strong negative voltages (Khan et al., 2008).

The model was used to estimate the transport rate of Cd^{2+} through $Ca_V3.1$ channels as a function of $[Cd^{2+}]_o$ (Fig. 8E). The model predicted that, with 3 to 10 nM Cd^{2+}, $Ca_V3.1$ channels could transport Cd^{2+} through an open channel at a

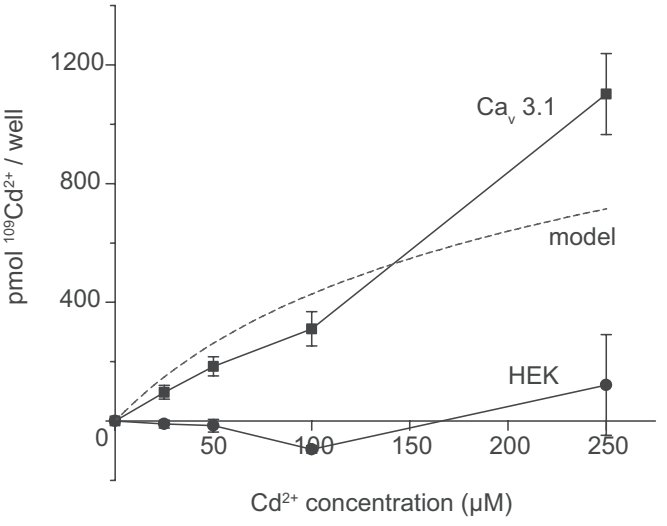

Fig. 7. Uptake of Cd^{2+} by HEK293 cells. NNC 55-0396 (25 μM)-sensitive uptake of $^{109}Cd^{2+}$ in untransfected HEK293 cells and HEK293 cells stably expressing $Ca_V3.1$ calcium channels is shown. Cells were incubated for 30 min with the indicated concentrations of Cd^{2+}. Dashed line, transport rate calculated with the two-binding site/three-barrier model, by using the assumptions described in the text (n = 5–9).

rate on the order of 1 Cd^{2+} ion/s. To evaluate the steady-state Cd^{2+} entry rate, the expected steady-state open probability (shown as a function of voltage in Fig. 8F) was calculated with the model described by Serrano et al. (1999). It should be noted that the window open probability is constant at depolarized potentials, because of incomplete inactivation.

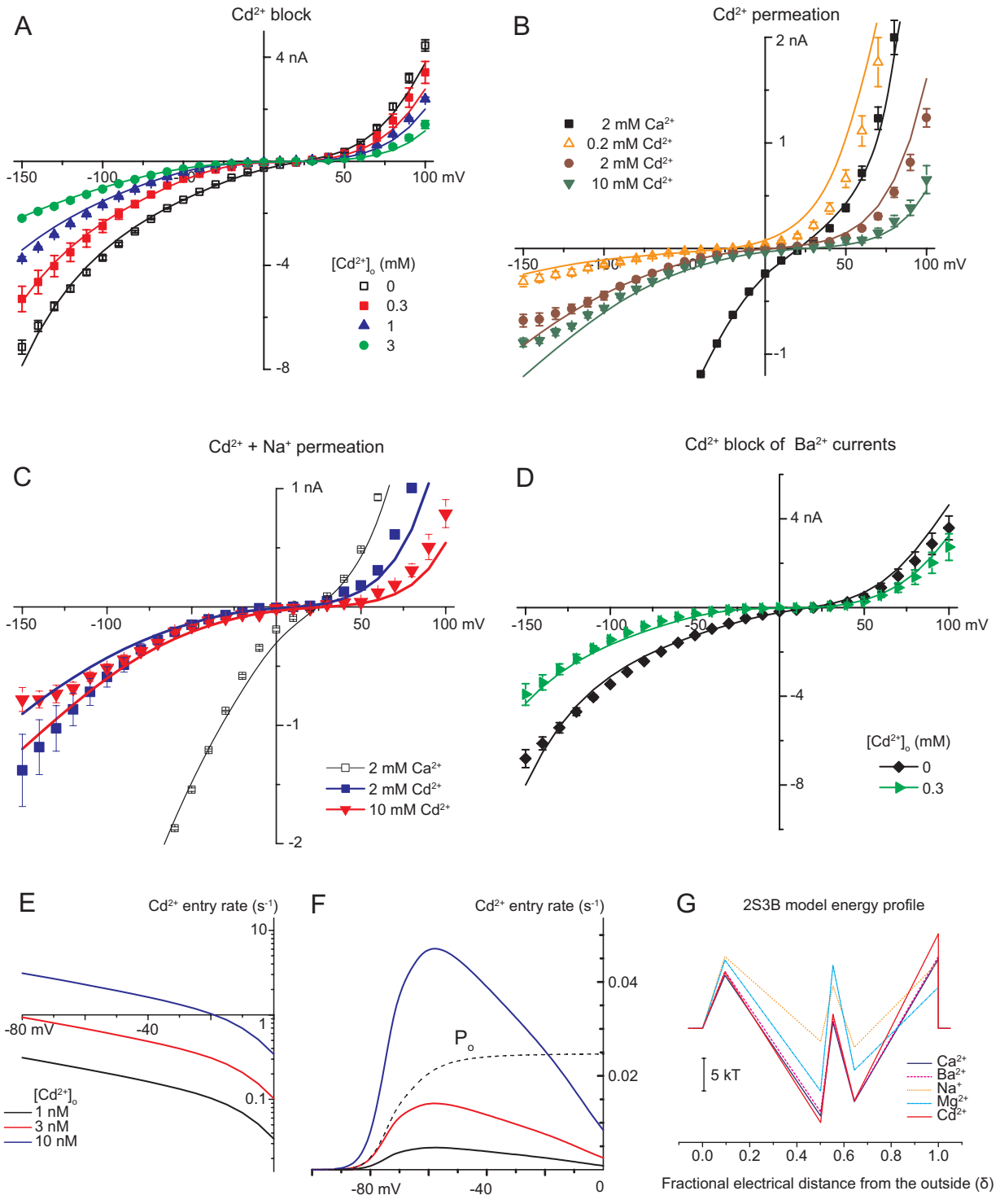

Fig. 8. Two-binding site/three-barrier Eyring rate model for Cd^{2+} block and permeation in $Ca_V3.1$ channels. A, fit of the model to II-V curves with extracellular Cd^{2+} added to solutions containing 2 mM Ca^{2+} (and extracellular and intracellular Na^+). B, fit to II-V curves in the absence of extracellular Ca^{2+} and Na^+. C, fit to II-V curves with extracellular Cd^{2+}, no extracellular Ca^{2+}, and normal extracellular Na^+ levels. D, fit to II-V curves with 2 mM extracellular Ba^{2+} and with added 0.3 mM extracellular Cd^{2+}. For A to D, symbols are experimental measurements and curves are model calculations. E, calculated rates of Cd^{2+} influx through an open $Ca_V3.1$ channel as a function of voltage for different $[Cd^{2+}]_o$ values. F, calculated rates of Cd^{2+} influx through the window current of Cav3.1 channels as a function of voltage (same symbols as E). Dashed line, open probability for Cav3.1, calculated with the model described by Serrano et al. (1999). G, energy profiles for the ions included in the model. The energy levels for Cd^{2+}, from outside to inside, are 8.56, −14.46, 2.17, −11.10, and 14.49 kT. Other parameters are from the report by Lopin et al. (2010).

Figure 8F also shows the transport rate through an open channel multiplied by the steady-state open probability; this is the calculated Cd^{2+} transport rate through the window current. The model could be compared directly with the incubation data by multiplying the transport rate by estimates for the number of cells per well (200,000 cells/well), the number of channels per cell (8000 channels/cell) (Lopin et al., 2010), and the open probability at rest, taking into account slow inactivation (0.975%), which was calculated by assuming 98.5% fast inactivation (Serrano et al., 1999) and 35% slow inactivation (Hering et al., 2004) at steady state. All values were determined at −35 mV (Chemin et al., 2000). As shown in Fig. 7, the uptake calculated from the model was very similar to the experimentally observed rate (see *Discussion*).

Shifts in Gating with Cd^{2+}. To determine whether Cd^{2+} affected gating, activation curves were calculated from the Cd^{2+} block data (Fig. 1) by using the relative open probability, which was calculated by dividing the I-V current by the II-V current at each voltage (Serrano et al., 1999) (Fig. 9B). This measurement could not be used for the Cd^{2+} permeation data, because the I-V currents were too small to be measured accurately (Fig. 6D); therefore, currents were measured from tail currents after brief (2-ms) depolarizations (Fig. 9A). Activation was shifted to more-positive voltages with 2 mM Cd^{2+}, compared with 2 mM Ca^{2+}. As described previously (Khan et al., 2008), Ca^{2+} causes a voltage shift by interacting with the negatively charged head groups on the cell membrane without binding, i.e., through charge screening or a Gouy-Chapman mechanism (Hille et al., 1975). The additional shift caused by Cd^{2+}, compared with an equimolar concentration of Ca^{2+}, requires some additional mechanism of action, most likely binding of Cd^{2+} to the channel or cell surface. The simplest such model is a Gouy-Chapman-Stern mechanism, which allows cations to bind to surface charges in addition to screening. The voltage shifts caused by Cd^{2+} are shown in Fig. 10. It can be seen that, with the use of $K_A = 0.44\ M^{-1}$, both the permeation and block data were described fairly well (Fig. 10). Binding to surface charges should shift the time constants for channel closing to the same degree as for the relative open probability data. The time constants for the tail currents of Ca^{2+} currents, and Ca^{2+} currents with the addition of Cd^{2+}, are shown in Fig. 9C. Cd^{2+} caused no change in the inactivation rate (e.g., above 0 mV). There was no clear shift in the voltage dependence of channel closing (e.g., below −50 mV), but there were slight changes in the slope with 1 or 3 mM Cd^{2+}. This indicates that the effects of Cd^{2+} on gating cannot be explained fully with the Gouy-Chapman-Stern theory. The effects of Cd^{2+} on $Ca_v3.1$ gating should be negligible at the Cd^{2+} concentrations found in the body.

Discussion

Cd^{2+} Permeation and Block. In this study, we demonstrate that Cd^{2+} can permeate directly through $Ca_V3.1$ calcium channels. The voltage dependence of Cd^{2+} block of Ca^{2+} currents strongly suggested that Cd^{2+} is a permeant ion, and inward currents were carried by Cd^{2+} in the absence of other extracellular permeant ions. To calculate the rate at which Cd^{2+} could permeate $Ca_v3.1$ channels at concentrations seen during Cd^{2+} exposure (3–10 nM), we used a model of permeation and estimated that ~1 Cd^{2+} ion/s could pass through an open channel.

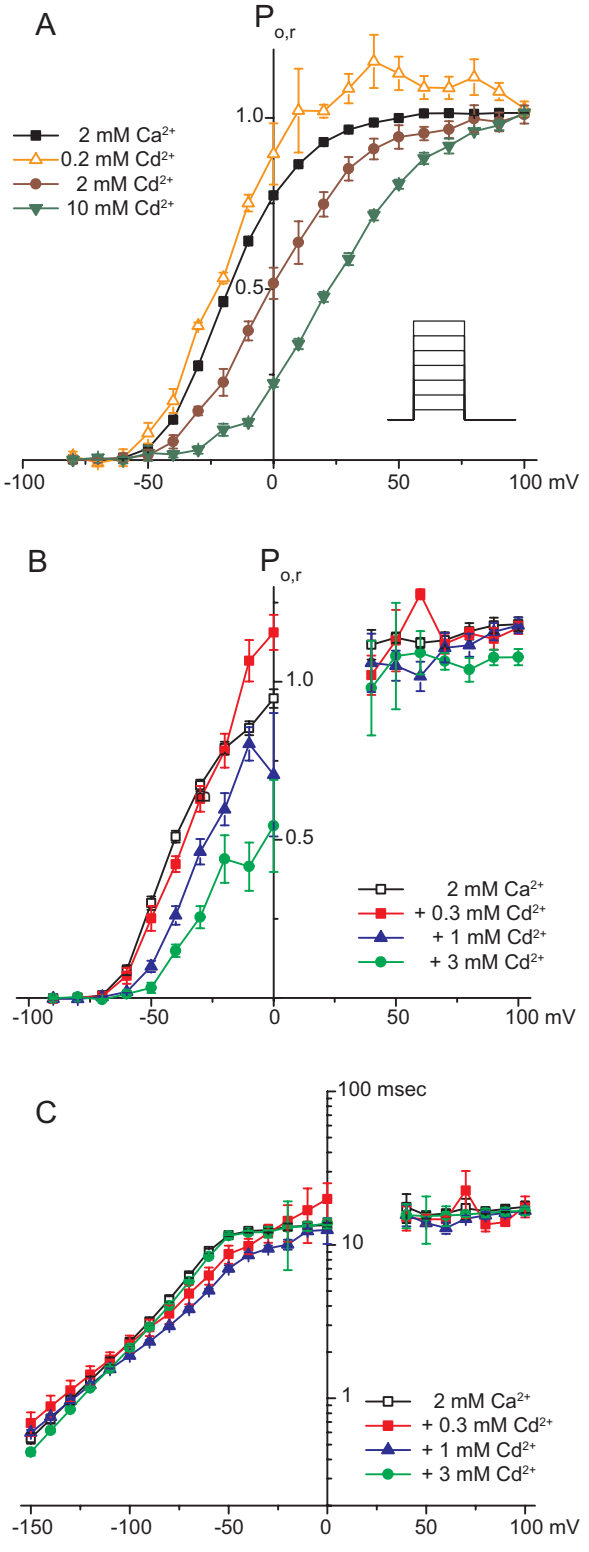

Fig. 9. Effects of Cd^{2+} on gating. A, activation measured from tail currents after 2-ms prepulses ($n = 4$), normalized to the tail currents after steps to 100 mV. B, activation curves calculated by dividing the peak I-V current by the II-V current ($n = 4$). C, time constants of the tail currents with the II-V protocol ($n = 4$). $P_{o,r}$, relative open probability.

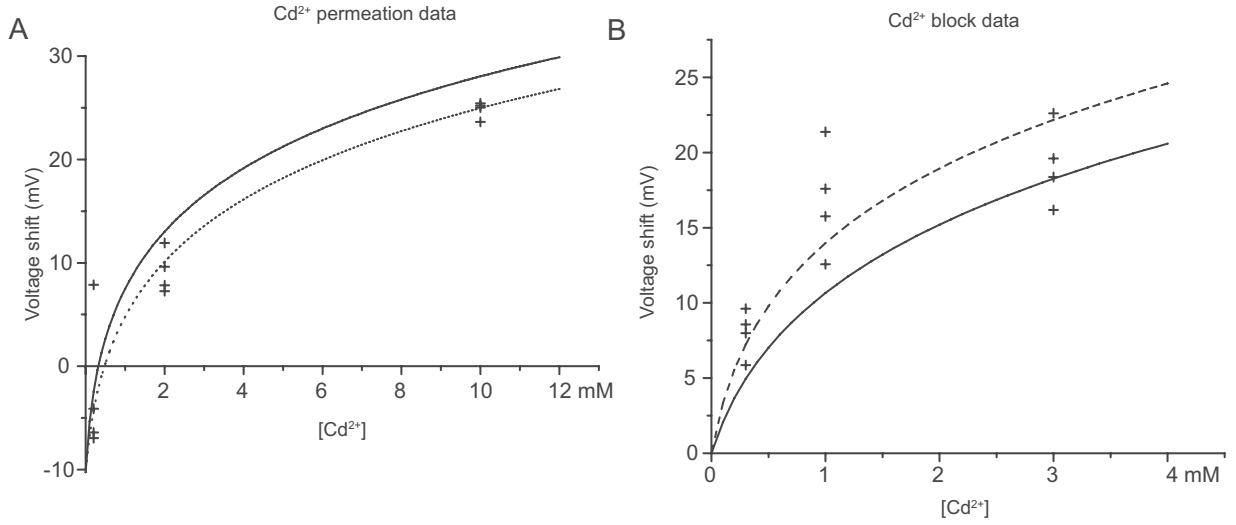

Fig. 10. Voltage shifts induced by Cd^{2+}, fitted to the Gouy-Chapman-Stern theory by using the Grahame equation. Solid curves, fits of Cd^{2+} block and permeation data to the same K_A (0.4435 M^{-1}). The fits were fairly good for both data sets, although different methods were used to measure the relative open probability ($P_{o,r}$) (Fig. 9). The best fits to the data sets separately yielded 0.85 M^{-1} for block and 0.26 M^{-1} for permeation (dashed curves).

Cd^{2+} is classically considered a calcium channel blocker, but previous studies demonstrated relief of block with hyperpolarization, which is strong evidence that Cd^{2+} can enter cells through voltage-dependent calcium channels (Brown et al., 1983). This is not surprising in principle, because many divalent cations (including Ca^{2+} itself) can act as either pore blockers or permeant cations, depending on conditions (Almers and McCleskey, 1984; Hess and Tsien, 1984). The size of currents carried by Cd^{2+} was surprising, however, i.e., 5 to 17% of the current carried by Ca^{2+}, with both ions at 2 mM (Fig. 6). On the basis of reversal potentials observed with Cd^{2+} (in the absence of Ca^{2+}), the permeability ratio was 0.66. It should be noted that the permeability ratio primarily reflects the strength of binding but the actual current observed is also affected by the rate of ion movement through the pore.

$Ca_V3.1$ block by Cd^{2+} decreased with hyperpolarization, which was the reverse of the voltage dependence observed for many other divalent cations, including Mg^{2+}, Co^{2+}, and Ni^{2+} (Serrano et al., 2000; Díaz et al., 2005; Obejero-Paz et al., 2008). This finding reflects the relatively strong permeation observed for Cd^{2+}. The relief of Cd^{2+} block with hyperpolarization also was seen for Ca^{2+} channels in chicken sensory neurons (Swandulla and Armstrong, 1989), which suggests that it might be a common feature of Ca^{2+} channels. Furthermore, data obtained with a range of Cd^{2+} concentrations indicated that Cd^{2+} block was saturated at 80 to 85% (Fig. 2) and Cd^{2+} did not completely block currents through $Ca_V3.1$ channels. The remaining current is carried in part by Cd^{2+} and in part by Ca^{2+}; our permeation model predicted that 50 to 60% of the inward current would be carried by Cd^{2+} with 2 mM Ca^{2+} and 3 mM Cd^{2+} in the extracellular solution.

It does not appear that the incomplete block of calcium channels by Cd^{2+} was noted previously. One factor is that most previous studies measured inhibition by using the I-V protocol, instead of the II-V protocol used here. Because Cd^{2+} shifts gating to more-positive voltages, inhibition measured with the I-V protocol would include both inhibition through pore block and inhibition through decreased channel open probability, which would exaggerate the potency of Cd^{2+} as a pore blocker and also might exaggerate the maximal extent of pore block (Fig. 1D).

In the experiments examining Cd^{2+} block of Ca^{2+} currents, the reversal potential was shifted to more-negative potentials with Cd^{2+}, which is opposite expectations based on the GHK theory. Deviations from GHK behavior are expected for multiple-ion pores such as calcium channels, for which ion-ion interactions are important.

Permeation Model. With the nanomolar concentrations observed with chronic Cd^{2+} exposure in vivo, the rate of Cd^{2+} permeation through $Ca_v3.1$ channels cannot be measured directly by using electrophysiological experiments. We estimated the transport rate by using the rate theory model of permeation in calcium channels described by Eyring (1935). The model we propose is a refinement of the original two-site/three-barrier models of calcium channels (Almers and McCleskey, 1984; Hess and Tsien, 1984) fit to a large data set involving various voltages and Ca^{2+}, Ba^{2+}, Mg^{2+}, and Na^{+} concentrations (Lopin et al., 2010). Parameters for Cd^{2+} were estimated by including our data on Cd^{2+} block and permeation. The model could then translate electrophysiological data into transport rates for trace metals through an ion channel under pathophysiological conditions.

The model was able to reproduce the $^{109}Cd^{2+}$ uptake data fairly well with the use of previously reported values for the window current and the membrane potential. Uncertainties in the resting potential of HEK293 cells, especially with $Ca_V3.1$ channels active (or partially blocked by Cd^{2+}), limit quantitative comparisons, but the fraction of $Ca_V3.1$ channels that are active at steady state near the assumed resting potential (−35 mV) (Chemin et al., 2000) does not depend strongly on voltage (Serrano et al., 1999).

Calcium Channels and Cd^{2+} Uptake. It is unlikely that there is a dedicated protein to transport Cd^{2+}, because it is not a biologically essential metal. Instead, Cd^{2+} is transported into cells through mechanisms used for other naturally occurring cations, such as Ca^{2+} (i.e., "ionic mimicry") (Clarkson, 1993; Bridges and Zalups, 2005). Cd^{2+} uptake

through $Ca_V3.1$ channels in our study (Fig. 7) is comparable to the findings of a previous study with ZIP14 (Girijashanker et al., 2008), but uncertainty in expression levels for different channels and transporters prevents definitive conclusions regarding the relative importance of pathways for Cd^{2+} influx. Previous studies also linked L-type calcium channels (Hinkle et al., 1987) and the calcium-selective transient receptor potential canonical 6 channel (Kovacs et al., 2011) to Cd^{2+} uptake. Development of resistance to Cd^{2+} in cell culture has been linked to down-regulation of $Ca_V3.1$, which suggests the involvement of this channel in Cd^{2+} toxicity (Leslie et al., 2006). Given the large number of calcium channels expressed throughout the body, the importance of Ca^{2+} signaling, and the large number of ions a channel can transport ($\sim 10^5$ ions/s), even slight permeability of a calcium channel to Cd^{2+} might lead to significant Cd^{2+} entry. This is especially true for $Ca_V3.1$, which has a substantial window current near the resting potential.

Acknowledgments

We thank Dr. Ed Perez-Reyes (University of Virginia) for the HEK293 cell line stably transfected with $Ca_V3.1$.

Authorship Contributions

Participated in research design: Lopin, Thévenod, and Jones.
Conducted experiments: Lopin, Thévenod, and Page.
Performed data analysis: Lopin, Thévenod, Page, and Jones.
Wrote or contributed to the writing of the manuscript: Lopin, Thévenod, and Jones.

References

Agency for Toxic Substances and Disease Registry (2008) *Toxicological Profile for Cadmium*, Centers for Disease Control and Prevention, Atlanta.
Almers W and McCleskey EW (1984) Non-selective conductance in calcium channels of frog muscle: calcium selectivity in a single-file pore. *J Physiol* **353:**585–608.
Andreasen D, Jensen BL, Hansen PB, Kwon TH, Nielsen S, and Skøtt O (2000) The α_{1G}-subunit of a voltage-dependent Ca^{2+} channel is localized in rat distal nephron and collecting duct. *Am J Physiol Renal Physiol* **279:**F997–F1005.
Bridges CC and Zalups RK (2005) Molecular and ionic mimicry and the transport of toxic metals. *Toxicol Appl Pharmacol* **204:**274–308.
Brown AM, Tsuda Y, and Wilson DL (1983) A description of activation and conduction in calcium channels based on tail and turn-on current measurements in the snail. *J Physiol* **344:**549–583.
Chemin J, Monteil A, Briquaire C, Richard S, Perez-Reyes E, Nargeot J, and Lory P (2000) Overexpression of T-type calcium channels in HEK-293 cells increases intracellular calcium without affecting cellular proliferation. *FEBS Lett* **478:**166–172.
Clarkson TW (1993) Molecular and ionic mimicry of toxic metals. *Annu Rev Pharmacol Toxicol* **33:**545–571.
Díaz D, Bartolo R, Delgadillo DM, Higueldo F, and Gomora JC (2005) Contrasting effects of Cd^{2+} and Co^{2+} on the blocking/unblocking of human Ca_V3 channels. *J Membr Biol* **207:**91–105.
Elinder CG, Friberg L, Lind B, and Jawaid M (1983) Lead and cadmium levels in blood samples from the general population of Sweden. *Environ Res* **30:**233–253.
Erfurt C, Roussa E, and Thévenod F (2003) Apoptosis by Cd^{2+} or CdMT in proximal tubule cells: different uptake routes and permissive role of endo/lysosomal CdMT uptake. *Am J Physiol Cell Physiol* **285:**C1367–C1376.
Eyring H (1935) The activated complex in chemical reactions. *J Chem Phys* **3:**107–115.
Frazier CJ, George EG, and Jones SW (2000) Apparent change in ion selectivity caused by changes in intracellular K^+ during whole-cell recording. *Biophys J* **78:**1872–1880.
Girijashanker K, He L, Soleimani M, Reed JM, Li H, Liu Z, Wang B, Dalton TP, and Nebert DW (2008) *Slc39a14* gene encodes ZIP14, a metal/bicarbonate symporter: similarities to the ZIP8 transporter. *Mol Pharmacol* **73:**1413–1423.
Grahame DC (1947) The electrical double layer and the theory of electrocapillarity. *Chem Rev* **41:**441–501.
Gunshin H, Mackenzie B, Berger UV, Gunshin Y, Romero MF, Boron WF, Nussberger S, Gollan JL, and Hediger MA (1997) Cloning and characterization of a mammalian proton-coupled metal-ion transporter. *Nature* **388:**482–488.
Hassler E, Lind B, and Piscator M (1983) Cadmium in blood and urine related to present and past exposure: a study of workers in an alkaline battery factory. *Br J Ind Med* **40:**420–425.
Hering J, Feltz A, and Lambert RC (2004) Slow inactivation of the $Ca_V3.1$ isotype of T-type calcium channels. *J Physiol* **555:**331–344.
Hess P and Tsien RW (1984) Mechanism of ion permeation through calcium channels. *Nature* **309:**453–456.
Hille B, Woodhull AM, and Shapiro BI (1975) Negative surface charge near sodium channels of nerve: divalent ions, monovalent ions, and pH. *Philos Trans R Soc Lond B Biol Sci* **270:**301–318.
Hinkle PM, Kinsella PA, and Osterhoudt KC (1987) Cadmium uptake and toxicity via voltage-sensitive calcium channels. *J Biol Chem* **262:**16333–16337.
Hodgkin AL and Huxley AF (1952) The components of membrane conductance in the giant axon of *Loligo*. *J Physiol* **116:**473–496.
Huang L, Keyser BM, Tagmose TM, Hansen JB, Taylor JT, Zhuang H, Zhang M, Ragsdale DS, and Li M (2004) NNC 55-0396 [(1*S*,2*S*)-2-(2-(*N*-[(3-benzimidazol-2-yl)propyl]-*N*-methylamino)ethyl)-6-fluoro-1,2,3,4-tetrahydro-1-isopropyl-2-naphtyl cyclopropanecarboxylate dihydrochloride]: a new selective inhibitor of T-type calcium channels. *J Pharmacol Exp Ther* **309:**193–199.
Hung YM and Chung HM (2004) Acute self-poisoning by ingestion of cadmium and barium. *Nephrol Dial Transplant* **19:**1308–1309.
Järup L and Akesson A (2009) Current status of cadmium as an environmental health problem. *Toxicol Appl Pharmacol* **238:**201–208.
Khan N, Gray IP, Obejero-Paz CA, and Jones SW (2008) Permeation and gating in $Ca_V3.1$ (α1G) T-type calcium channels effects of Ca^{2+}, Ba^{2+}, Mg^{2+}, and Na^+. *J Gen Physiol* **132:**223–238.
Kovacs G, Danko T, Bergeron MJ, Balazs B, Suzuki Y, Zsembery A, and Hediger MA (2011) Heavy metal cations permeate the TRPV6 epithelial cation channel. *Cell Calcium* **49:**43–55.
Lacinová L, Klugbauer N, and Hofmann F (2000) Regulation of the calcium channel α_{1G} subunit by divalent cations and organic blockers. *Neuropharmacology* **39:**1254–1266.
Leclerc M, Brunette MG, and Couchourel D (2004) Aldosterone enhances renal calcium reabsorption by two types of channels. *Kidney Int* **66:**242–250.
Leslie EM, Liu J, Klaassen CD, and Waalkes MP (2006) Acquired cadmium resistance in metallothionein-I/II(−/−) knockout cells: role of the T-type calcium channel Cacna$_{1G}$ in cadmium uptake. *Mol Pharmacol* **69:**629–639.
Liu Z, Li H, Soleimani M, Girijashanker K, Reed JM, He L, Dalton TP, and Nebert DW (2008) Cd^{2+} versus Zn^{2+} uptake by the ZIP8 HCO_3-dependent symporter: kinetics, electrogenicity and trafficking. *Biochem Biophys Res Commun* **365:**814–820.
Lopin KV, Obejero-Paz CA, and Jones SW (2010) Evaluation of a two-site, three-barrier model for permeation in $Ca_V3.1$ (α1G) T-type calcium channels: Ca^{2+}, Ba^{2+}, Mg^{2+}, and Na^+. *J Membr Biol* **235:**131–143.
Obejero-Paz CA, Gray IP, and Jones SW (2008) Ni^{2+} block of $Ca_V3.1$ (α1G) T-type calcium channels. *J Gen Physiol* **132:**239–250.
Okubo M, Yamada K, Hosoyamada M, Shibasaki T, and Endou H (2003) Cadmium transport by human Nramp 2 expressed in *Xenopus laevis* oocytes. *Toxicol Appl Pharmacol* **187:**162–167.
Perez-Reyes E (2003) Molecular physiology of low-voltage-activated T-type calcium channels. *Physiol Rev* **83:**117–161.
Serrano JR, Dashti SR, Perez-Reyes E, and Jones SW (2000) Mg^{2+} block unmasks Ca^{2+}/Ba^{2+} selectivity of α1G T-type calcium channels. *Biophys J* **79:**3052–3062.
Serrano JR, Perez-Reyes E, and Jones SW (1999) State-dependent inactivation of the α1G T-type calcium channel. *J Gen Physiol* **114:**185–201.
Swandulla D and Armstrong CM (1989) Calcium channel block by cadmium in chicken sensory neurons. *Proc Natl Acad Sci USA* **86:**1736–1740.
Thévenod F (2010) Catch me if you can! Novel aspects of cadmium transport in mammalian cells. *Biometals* **23:**857–875.
Williams SR, Tóth TI, Turner JP, Hughes SW, and Crunelli V (1997) The 'window' component of the low threshold Ca^{2+} current produces input signal amplification and bistability in cat and rat thalamocortical neurones. *J Physiol* **505:**689–705.
Zhou W and Jones SW (1995) Surface charge and calcium channel saturation in bullfrog sympathetic neurons. *J Gen Physiol* **105:**441–462.

Address correspondence to: Stephen W. Jones, Department of Physiology and Biophysics, Case Western Reserve University, Cleveland, OH 44106. E-mail: swj@case.edu